Heat Mass Transfer (2018) 54:831–839
DOI 10.1007/s00231-017-2181-6

ORIGINAL

Numerical model for the thermal behavior of thermocline storage tanks

Ismael A. S. Ehtiwesh[1,2] · **Antonio C. M. Sousa**[1]

Received: 25 January 2017 / Accepted: 27 September 2017 / Published online: 5 October 2017

Abstract Energy storage is a critical factor in the advancement of solar thermal power systems for the sustained delivery of electricity. In addition, the incorporation of thermal energy storage into the operation of concentrated solar power systems (CSPs) offers the potential of delivering electricity without fossil-fuel backup even during peak demand, independent of weather conditions and daylight. Despite this potential, some areas of the design and performance of thermocline systems still require further attention for future incorporation in commercial CSPs, particularly, their operation and control. Therefore, the present study aims to develop a simple but efficient numerical model to allow the comprehensive analysis of thermocline storage systems aiming better understanding of their dynamic temperature response. The validation results, despite the simplifying assumptions of the numerical model, agree well with the experiments for the time evolution of the thermocline region. Three different cases are considered to test the versatility of the numerical model; for the particular type of a storage tank with top round impingement inlet, a simple analytical model was developed to take into consideration the increased turbulence level in the mixing region. The numerical predictions for the three cases are in general good agreement against the experimental results.

Highlights
- Predictions and experiments present similar trend for the time evolution.
- Inlet region deviations are most likely due to the high-level of turbulence.
- The ad-hoc proposed turbulence model leads to improved predictions.
- Predictions in relation to the experiments, have a maximum deviation of less than 12%.

✉ Ismael A. S. Ehtiwesh
ehtiwesh@gmail.com

Antonio C. M. Sousa
antoniosousa@ua.pt

[1] Department of Mechanical Engineering, Centre for Mechanical Technology and Automation, University of Aveiro, Campus Universitário de Santiago, 3810-193 Aveiro, Portugal

[2] Department of Mechanical Engineering, Faculty of Engineering, Sabratha University, Sabratha, Libya

Abbreviations

List of symbols

a	Fitting constant [m^{-1}]
a_w	Ratio between thermal losses area and tank volume [m^{-1}]
C	Specific heat capacity [J/kg-K]
d	Exit diameter [m]
D	Diameter [m]
h_w	Coefficient of thermal losses to the surrounding [W/m^2-K]
h_v	Volumetric interstitial heat transfer coefficient [W/m-K]
k	Thermal conductance [W/m-K]
l_{mix}	Mixing length [m]
L	Height of the tank [m]
$\dot{m}$	Mass flow rate [m^3/s]
Pr_t	Turbulent Prandtl number
r	Radius [m]
t	Time [s]
T	Temperature [K]
u	Velocity [m/s]
U	Average exit velocity [m/s]
V	Volume [m^3]
x	Downstream distance [m]

Greek letters

α	Thermal diffusivity [m^2/s]
ε	Porosity of the storage medium (void fraction)

ν_f	Kinematic viscosity [m^2/s]
ν_t	Kinematic eddy viscosity [m^2/s]
ν_{total}	Effective viscosity [m^2/s]
	Dimensionless temperature
ρ	Density [kg/m^3]
σ	Standard deviation related to the spread of the profile across the centerline
δ	Distance from the centerline to the edge of the spreading [m]

Subscripts

*	Subscript indicating dimensionless quantities
eff	Subscript refering to the effective storage medium
f	Fluid
m	Momentum
s	Solid
t	Turbulent
w	Water
ZEF	Zone of flow establishment

1 Introduction

CSPs, despite their promise, still face major technological challenges; in contrast to totally *dispatchable* fossil sources, CSPs are an incomplete energy resource depending on the hourly and daily supply of solar radiation; this radiation is variable and may not suffice for power generation. In view of these constraints, the long-term strategy for CSPs is to have them fully integrated into a power grid with adequate adaptation to auxiliary facilities, generator mix, including variable generation sources such as wind and even solar photovoltaics. Otherwise, to extend their power production time range without power back-up, the use of storage systems is required, of which the thermal energy storage (TES) system is the most common one. These systems are charged when solar irradiation is available, and the stored energy will be released at night or when there is not sufficient solar irradiation, and in the event of a peak of energy demand. Consequently, TES systems have a major role in CSPs by extending their availability in terms of power production; their development however, depends on different technological issues ranging from materials [1] to operational strategies [2]. CSPs, when using TES systems, provide for *dispatchable* renewable energy, and they consist of three essential components - the power block, the solar field, and the thermal storage; these components are independent but interrelated, and they can be sized based on different criteria [3]. CSPs with large storage capacity may be able to generate base-load solar electricity day and night and, depending on the carbon taxes in place, make them economically competitive with fossil fuel power plants with high emission levels of greenhouse gases [4].

Thermocline systems have the potential of providing extended storage capability at reduced cost, when compared to two-tank systems; as a consequence, thermocline technology has been receiving increased worldwide attention. However, large-scale utilization of the thermocline system is still hindered by several technical problems, among them time-dependence of temperature delivery and sizing requirements. The thermocline tank, as compared to other storage systems, such as the two-tank technologies, has the potential of reducing the capital cost, on average, by 24%; however, for large single-tank installations the cost abatement can be as high as 33% [5].

There are several studies [2, 6–12] that aim to integrate the thermocline storage tank with solar thermal systems, which, in general, examine the effect of varying different system parameters such as porosity, filler material characteristics, tank dimensions on overall performance of the thermal storage systems. Most of these studies perform the analysis of thermocline storage tanks by considering packed-bed systems, and the numerical formulation is based on Schumann's one-dimensional model [13]. The model includes two heat transfer equations, when fluid and packed-bed filler particles are at different temperatures. For the particular case of liquid heat transfer fluids, some of the above-mentioned studies indicate that the difference between fluid and solid filler temperatures is small, because of the high overall heat transfer coefficient between fluid and solid filler [2]. Under these conditions, it can be assumed that liquid and filler are at the same temperature; hence, a single-phase model can be formulated, for which only one heat transfer equation is required. Tesfay and Venkatesan [6] proposed a one-dimensional model based on the Schumann equations and assuming constant thermophysical properties for the heat transfer fluid (HTF) and no heat loss to the environment. The study of Bayon and Rojas [2], which is based on a single phase one-dimensional model, conducts a parametric analysis, in which the relative importance of various design parameters is established. They consider the HTF and the filler bed at the same temperature, which implies that they are in thermal equilibrium. By contrast, a detailed two-temperature, two-dimensional model was presented by Yang and Garimella [7, 8]; they studied the discharge process of the thermocline system with molten salt and filler material and the effect of non-adiabatic boundaries on the thermal performance of thermocline tanks. Flueckiger et al. [9], by using a comprehensive thermomechanical model, carried out an analysis for thermal ratcheting - a phenomenon involving the tank walls, which is caused by temperature variations and the settling of the filler particles. Xu et al. [10] studied the heat transfer and fluid dynamics in the thermocline storage system using a two-dimensional and two-phase (solid-fluid) model. Particular emphasis was given to the influence of the interstitial heat transfer rate and the filler thermal conductivity, and they concluded that a uniform cross-sectional temperature could be achieved with two insulation layers, and the thermocline region can cover more than one-third of the tank height at maximum thickness

for a tank height of 14 m. The same authors also investigated the effect of the fluid inlet velocity, inlet temperature, porosity, tank height and solid particle properties on the thermal performance of the TES system [11, 12].

In the present study, a numerical model for thermal storage systems was developed aiming to simulate their behavior efficiently and with minor computing requirements having in this way the potential of enabling enhancement of effectiveness, economics and operational characteristics of CSPs. Charging stages were comprehensively simulated and analyzed with particular emphasis on heat transfer and fluid dynamics within the thermocline storage system. The numerical investigation is carried out for three different cases, namely: a) top round impingement inlet tank with no filler, which was studied experimentally by Zurigat et al. [14], b) Sandia Laboratory (SL) prototype, as described in [15] and c) Solar One tank (SO) analyzed experimentally in [16]. The predictions are compared against the experimental data and, as indicated by the results, with very promising results.

2 Methodology

The numerical model aims the dual-purpose of describing the behavior of a particular type of TES system with particular emphasis on the time-dependent outlet temperature while allowing the straightforward implementation of a code used for simulating the annual performance of CSPs. Therefore the numerical model will employ a set of governing equations which economically and accurately can characterize the dominant energy transfer mechanisms in the charging phase of the thermocline storage tank. The packed bed filler is characterized by a void fraction ε [17]:

$$\varepsilon = V_f/\left(V_f + V_s\right) \tag{1}$$

Where V_f and V_s are the free space and solid filler volumes, respectively; the HTF flows through the free space. The energy balances are written in one dimension assuming that the significant temperature variation only occurs in the vertical axial direction z. The governing equations of the HTF and packed bed are those proposed by Schumann [13], namely:

$$\rho_f C_f \varepsilon \frac{\partial T_f}{\partial t} + \left(\dot{m} C_f/A\right)\frac{\partial T_f}{\partial z} = h_v\left(T_s - T_f\right) \tag{2}$$

$$\rho_s C_s (1-\varepsilon)\frac{\partial T_s}{\partial t} = h_v\left(T_f - T_s\right) \tag{3}$$

Where T_f and T_s are the temperatures of the fluid and particles, respectively. The heat transfer between the HTF and the packed bed is accounted by a volumetric interstitial heat transfer coefficient h_v, which appears on the right-hand side of Eqs. (2) and (3). However, based on the available literature [18], the Biot number is sufficiently small to consider uniform temperature for the particles and the Nusselt number is large enough to assume that fluid and particles are in thermal equilibrium; consequently, the energy balance equation for the HTF and particles within the thermocline system that describes the storage system is written as follows:

$$(\rho C)_{eff}\frac{\partial T}{\partial t} + \varepsilon(\rho C)_f u_f \frac{\partial T}{\partial z} = k_{eff}\frac{\partial^2 T}{\partial z^2} - h_w a_w (T - T_w) \tag{4}$$

The thermal loss from the fluid to the tank wall expressed by the term "$h_w a_w$(T-T_w)" is being neglected because the outside wall of the tank is assumed to be well insulated, for instance an fiberglass blanket insulation (~0.035 W/m-K) with 0.05 m thickness yields a typical reduction in heat loss of nearly 90%; therefore, the main contribution to temperature variation with time and position is the movement of the thermocline zone. Equation (4) with this simplification becomes:

$$(\rho C)_{eff}\frac{\partial T}{\partial t} + \varepsilon(\rho C)_f u_f \frac{\partial T}{\partial z} = k_{eff}\frac{\partial^2 T}{\partial z^2} \tag{5}$$

The heat transfer equation is expressed in dimensionless coordinates aiming the simplification of the solution procedure and to obtain general results in terms of performance parameters; consequently, all variables are expressed in dimensionless form by using the following normalization:

$$z^* = z/L \tag{6}$$

$$t^* = t\alpha_{eff}/L^2 \tag{7}$$

$$u^* = \varepsilon(\rho C)_f L u_f / k_{eff} \tag{8}$$

$$\theta = T - T_{min}/(T_{max} - T_{min}) \tag{9}$$

The effective thermal diffusivity α_{eff} is defined as follows:

$$\alpha_{eff} = k_{eff}/(\rho C)_{eff} \tag{10}$$

Where the effective thermal conductivity k_{eff} and the effective product of density and specific heat, $(\rho C)_{eff}$, are formulated as follows:

$$k_{eff} = \varepsilon k_f + (1-\varepsilon)k_s \tag{11}$$

$$(\rho C)_{eff} = \varepsilon(\rho C)_f + (1-\varepsilon)(\rho C)_s \tag{12}$$

With constant diffusion coefficients, the resulting dimensionless governing equation becomes:

$$\frac{\partial \theta}{\partial t^*} + u^*\frac{\partial \theta}{\partial z^*} = \frac{\partial^2 \theta}{\partial z^{*2}} \tag{13}$$

For the numerical solution of Eq. (13), the tank is discretized in a predetermined number of non-overlapping control volumes and each height position at a temperature $_i$ is represented by a spatial node Z^*_i. The finite control volume

method [19, 20] with a linear interpolation is used to discretize Eq. (13); in addition, the discretized adjective term is approximated by a first-order upwind scheme and it is used a time implicit scheme. Formally, assuming the coefficients constant, the discretized equation is formulated as follows:

$$-\left(\frac{\Delta t^*}{\Delta z^{*2}}+\frac{u^*\Delta t^*}{\Delta z^*}\right)\theta_{z-1}^{t+1}+\left(1+\frac{2\Delta t^*}{\Delta z^{*2}}+\frac{u^*\Delta t^*}{\Delta z^*}\right)\theta_z^{t+1}-\left(\frac{\Delta t^*}{\Delta z^{*2}}\right)\theta_{z+1}^{t+1}=\theta_z^t \tag{14}$$

For each time step, the set of algebraic equations is solved by using the tri-diagonal matrix algorithm (TDMA) within the Matlab environment.

3 Case studies

The numerical code was developed to systematically investigate the behavior of different thermocline energy storage systems was extensively tested in terms of solution accuracy and mesh convergence [3]. In addition, the code was compared with a version using a time explicit scheme; although the predictions are similar, the implicit version of the code shows a marked reduction (~20%) in terms of CPU time because it does not have the time step stability limitation of the explicit version; however, for too large time steps (larger than 5 to 6 times the maximum explicit time step), the implicit solution accuracy may start to deteriorate. In order to validate the numerical model, comparisons were conducted for three particular types of thermocline tanks for which experimental data sets are available in the literature.

As it will be discussed in Section 4, predictions present significant deviations from the experimental data, in particular for the mixing region close to the inlet. These deviations were postulated to be due to the high-level of turbulence in this region due to the localized high level of mixing. Therefore, one possible way of taking into consideration the effect of turbulence is using a scaled mixing length formulation, which is based on the velocity profile. A suitable mixing length model may be capable of predicting the temperature time development along the downstream direction of the flow. The effective viscosity ν_{total} is given by Eq. (15), where the turbulent kinematic viscosity ν_t is equal to zero at the steady state zones for the undisturbed region, i.e., in this region the effective viscosity is constant and equal to the kinematic viscosity ν_f.

$$\nu_{total}=\nu_f\left(1+\nu_t/\nu_f\right) \tag{15}$$

The turbulent diffusivity α_t will be calculated based on the kinematic eddy viscosity ν_t, by assuming the turbulent Prandtl number Pr_t has a constant value; therefore

$$\alpha_t=\nu_t/Pr_t \tag{16}$$

The normalized governing Eq. (13) becomes:

$$\frac{\partial\theta}{\partial t^*}+u^*\frac{\partial\theta}{\partial z^*}=\frac{\partial}{\partial z^*}\left[\left(1+\varepsilon\frac{k_f\ \alpha_t}{k_{eff}\,\alpha_f}\right)\frac{\partial\theta}{\partial z^*}\right] \tag{17}$$

Under these conditions the objective is to determine an appropriate relation for the eddy diffusivity. The procedure involves the following steps:

1) Calculate the inlet value of the eddy viscosity using the mixing length theory with the assumption the inflow behaves as a submerged round jet; and
2) Determine a damping function as a function of the distance away from the inlet.

The description of a submerged turbulent round jet proposed by Cushman-Roisin [21] is followed for the simplified representation of a turbulent round jet penetrating a fluid at rest, Fig. 1.

The spreading is linear with the distance away from the inlet and the cross-jet velocity profiles, with the exception of that at the inlet are similar one to another, where the virtual source is at x = 0. It should be noted that there is a universal angle of 11.8° yielding, since *tan(11.8°) ≃ 1/5*, the relation between the jet radius and the downstream distance x from the virtual source is:

$$\delta(x)=x/5 \tag{18}$$

Where $\delta(x)$ is the distance from the centerline to the edge of the spreading. The initial jet radius is equal to half the exit diameter d; therefore, the distance x must be counted from a distance *5d/2* into the conduit, which is known as virtual source [21]. The velocity profile across the jet presents a nearly Gaussian shape, which can be written as:

$$u(x,r)=u_{max}exp\left(-r^2/2\sigma^2\right) \tag{19}$$

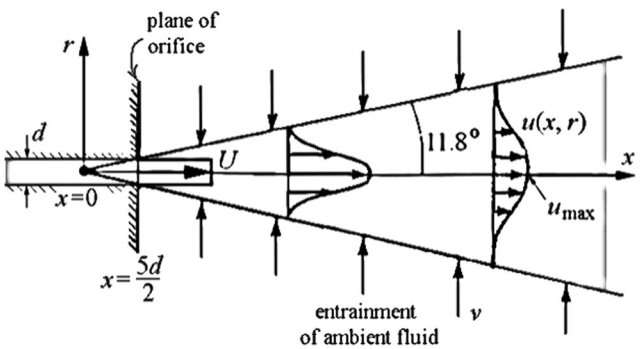

Fig. 1 Simplified representation of a turbulent round jet penetrating a fluid at rest. The spreading is linear with the distance away from the inlet and the cross-jet velocity profiles, with the exception of that at the inlet are similar one to another [21]

Where x is the downstream distance along the jet (counted from the virtual source), r is the cross-jet radial distance from its centerline, $u_{max}(x)$ is the maximum speed at the centerline, and $\sigma(x)$ is the standard deviation related to the spread of the profile across the centerline. The value of σ is equal to $x/10$ [21], and Eq. 18 can be rewritten as:

$$u(x,r) = u_{max} exp\left(-50r^2/x^2\right) \tag{20}$$

In [21] the relations for maximum velocity u_{max} and the average velocity $\bar{u}$, respectively, are as follows:

$$u_{max} = (5d/x)U \tag{21}$$

and

$$\overline{u} = (5d/2x)U \tag{22}$$

Where U and d are the average axial velocity and the exit diameter, respectively. Therefore, the velocity along the centerline of the jet decreases inversely with the distance from the virtual source (i.e. the ratio U/u_{max} increases linearly with distance). Taking the mixing length hypothesis leads to the formulation of the kinematic eddy viscosity [22]:

$$\nu_t = l_{mix}^2 |\partial u/\partial r| \tag{23}$$

Where l_{mix} is the mixing length; and introducing $\partial u/\partial r$, which is derived from Eq. 20, into Eq. 23, it results:

$$\nu_t = l_{mix}^2 u_{max}\left(100r/x^2\right) exp\left(-50r^2/x^2\right) \tag{24}$$

Considering the aim is to develop a one-dimensional turbulence closure, in Eq. 24 the radial position r will be taken at $\delta(x)$ leading to:

$$\nu_t = l_{mix}^2 u_{max}\left(100\delta(x)/x^2\right) exp\left(-50\delta(x)^2/x^2\right) \tag{25}$$

Taking the relation given in [22] between l_{mix} and $\delta(x)$

$$l_{mix} = \xi\delta(x) \tag{26}$$

into Eq. 25, it results

$$\nu_t = (\xi\delta)^2 u_{max} 100\delta/x^2 exp\left(-50\delta^2/x^2\right) \tag{27}$$

Where ξ is a constant equal to 0.08 [22]. By introducing the relations for $\delta(x)$ and u_{max} into Eq.27, it yields

$$\nu_t = (\xi\, x/5)^2 (5d/x)U\left(100(x/5)/x^2\right) exp\left(-50(x/5)^2/x^2\right) \tag{28}$$

or

$$\nu_t = 0.0035dU \tag{29}$$

Therefore with a value of Pr_t equal to 0.9, the thermal diffusivity is

$$\alpha_t = 0.0039dU \tag{30}$$

This relation for α_t is a constant value along the axis of the jet; and several time-dependent simulations indicate that is suitable for the inlet mixing region; however, it predicts poorly outside this region. Under these circumstances, it is proposed to introduce an exponential decay of α_t as a function of x. Similarly to the Van Driest damping function [23], although this physical situation is different, the model takes the following form:

$$\alpha_t = 0.0039dU exp(-\mathrm{a}x) \tag{31}$$

Where a is a fitting constant designed to have the value of α_t reduced to 10% of its original value at the end of the zone of flow establishment (ZFE). According to [24], the length of the zone of flow establishment, x_{ZFE}, is

$$x_{ZFE} = K_1 d \tag{32}$$

Where K_1 is a constant and equal to 5.1 [24]. If z is the distance away from the inlet, then

$$z_{ZFE} = K_1 d - 5d/2 \tag{33}$$

The resulting equation using the distance away from the inlet and based on Eq. 32 is

$$\alpha_t = 0.0039dU exp(-50z) \tag{34}$$

The effect of thermal diffusivity reflects reasonably well to the presence of turbulences caused by the mixing originating from the tank inflow. As the thermal diffusivity depends on the velocity, both will decrease with the distance traveled by the fluid away from the tank inlet.

a) Top, round impingement inlet tank with no filler

The numerical investigation carried out follows largely that carried out in [2], and it examines the thermocline thickness and effectiveness as a function of the thermocline motion, effective thermal diffusivity and height of the tank. The model was first validated with the experimental data presented by Zurigat et al. [14] and, in particular, for the top, round impingement inlet, which is the most challenging case. The tank shown in Fig. 2 has 0.4064 m in diameter, 1.4465 m in height and impingement inlet diameter of 0.018 m; the tank is filled only with water; therefore, the porosity takes the value of 1. The flow rate considered in this study is 0.098 kg-s^{-1}.

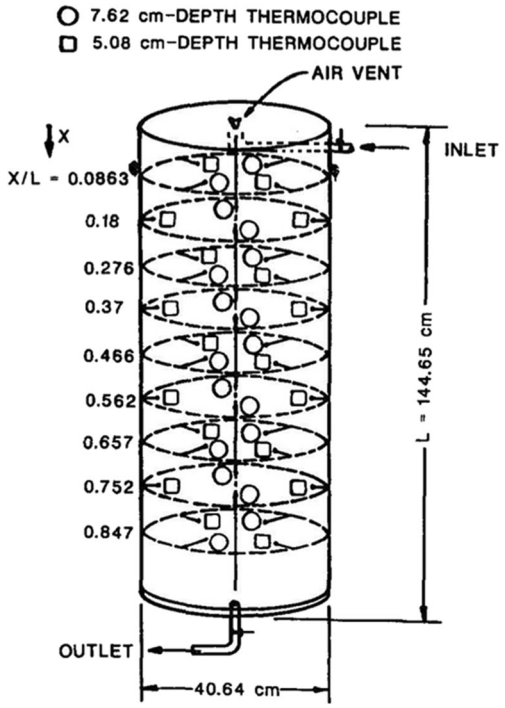

Fig. 2 Thermocouples layout of the experimental setup for hot-cold water system with central impingement inlet [14]

b) Sandia Laboratory (SL) prototype

The SL prototype [15] is a carbon steel tank, 6.1 m height and 3 m diameter with molten salts and a packed-bed of quartzite rock and silica filter sand. A thermocouple tree was placed in the middle with thermocouples every 0.15 m, vertically; they were placed on three radial arms each at 0.36 m, 3.05 m, and 4.88 m from the bottom. The tank has a radial flow distribution manifold at 0.1 m from the bottom that connects to a standpipe, housing the cold pump. The hot pump was supported from below with the salt pump from the top. The experimental results correspond to transient temperature profiles with minimum temperature equal to 289 °C and the maximum temperature 395.5 °C.

c) Solar One (SO) tank

The 170 MWht thermocline system of Solar One pilot plant tank [16, 18], and it is an industrial-scale thermal energy storage

Table 1 Characteristics of SL and SO tanks

Parameters	SL	SO
Energy	2.3 MWh_t	170 MWh_t
Discharge time	3 h	8 h
Porosity	0.22	0.22
Particle diameter	0.019 m	0.0046 m
HTF flow rate	5.46 kg-s^{-1}	23 kg-s^{-1}

Table 2 Thermal properties of HTF and filler materials [18]

HTF	Filler materials	
Solar salt	Quartzite rock and sand	
$\rho = 2090–0.636\ T$	$\rho = 2500$	kg-m^{-3}
$C_p = 1443 + 0.172\ T$	$C_p = 830$	J-kg^{-1}-K^{-1}
$k = 0.43 + 0.00019\ T$	$k = 5.69$	W-m^{-1}-K^{-1}
Caloria HT43 synthetic oil	Granite rock and sand	
$\rho = 87.1–0.713\ T$	$\rho = 2643$	kg-m^{-3}
$C_p = 1836.8 + 3.456\ T$	$C_p = 1020$	J-kg^{-1}-K^{-1}
$k = 0.125 + 0.00014\ T$	$k = 2.2$	W-m^{-1}-K^{-1}

of its kind, with 12 m in height and 18.2 m in diameter, and is made of carbon steel. To reduce heat losses to the ambient, the steel shell is covered by a 0.3 m layer of fiberglass insulation, while the top by a 0.6 m layer of calcium silicate [25]. The tank is filled with a packed-bed of sand and granite rock along the tank axis with a void fraction of 0.22, and Caloria HT-43 synthetic oil working between 179 °C and 295 °C.

The characteristics of SL and SO tanks are listed in Table 1, and the thermal and thermo physical properties of the HTF and solid filler materials are reported in Table 2.

4 Results and discussion

In case a), top, round impingement inlet tank with no filler; the predictions with the model without the ad-hoc turbulence closure developed in the previous section are compared against the experimental data in Fig. 3 for the charging phase. The experimental results correspond to transient temperature profiles with minimum and maximum temperatures equal to 25.9 °C and 50.8 °C, respectively.

The predictions show good agreement for the temporal data of the experiments, particularly for regions away from the top-

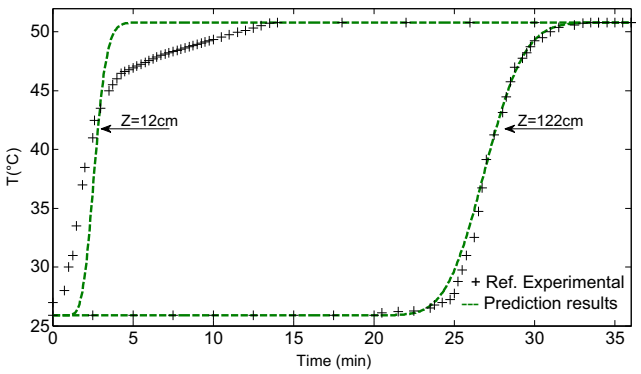

Fig. 3 Transient temperature profiles at two different locations in the charging process, initially discharged at a minimum temperature of 25.9 °C; comparison of the numerical model predictions against the experimental data taken from [2]

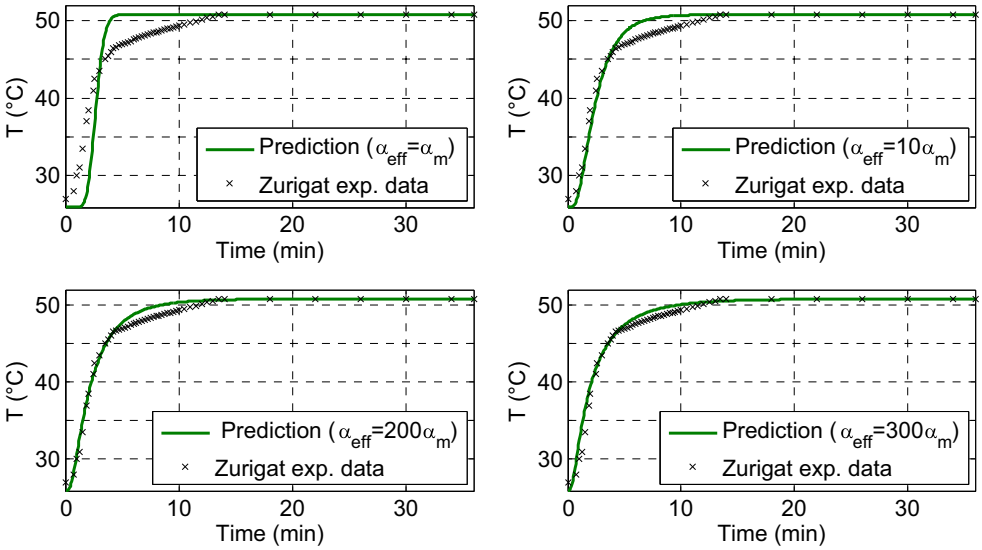

Fig. 4 Predicted temporal temperature development for different values of the effective thermal diffusivity at the inlet, location z = 0.12 m against Zurigat experimental data [2]

inlet region. The deviation near the inlet region, as already mentioned, is most likely due to the high-level of turbulence, where the main mechanism of heat transfer deeper is turbulent mixing; therefore, this discrepancy between predictions and experimental data in this region should not be surprising. There are possible avenues to take into account the presence of turbulence in the inlet region. In the present study, the objective is to improve the prediction capability of the model in the inlet region with minimal complexity and increase in computational effort. Under these circumstances, one possible formulation relies on the mixing length relations for a round jet as a case study, in which the underlying assumption is that whenever a moving fluid enters a quiescent body of the same fluid, a velocity shear is created between the entering and ambient fluids, causing turbulence and mixing. The turbulence characteristics greatly depend on the geometry of the flow domain; therefore, particular consideration should be given to this particular constraint. In addition, it is postulated that the mismatch between predicted and experimental temperature profiles observed in the inlet region is due to local turbulence enhancement; to test this assertion, different values for the effective thermal diffusivity are considered to describe the heat transport behavior. The effective diffusivity is equal to the summation of turbulent diffusivity and momentum diffusivity as shown in Eq. (15). Figures 4 and 5 report the impact of changing the effective diffusivity at the inlet and outlet zones. The effective diffusivity is tested for values 1, 10, 200 and 300 times, respectively, that of the momentum diffusivity for the location at the vicinity of the entering zone at z equal to 0.12 m; while, the effective diffusivity at z equal to 1.22 m is 1, 2, 3 and 4 times, respectively, of the momentum diffusivity. At the inlet zone, the value of the effective diffusivity that leads to the best agreement with the experimental data is approximately 300 times the momentum diffusivity,

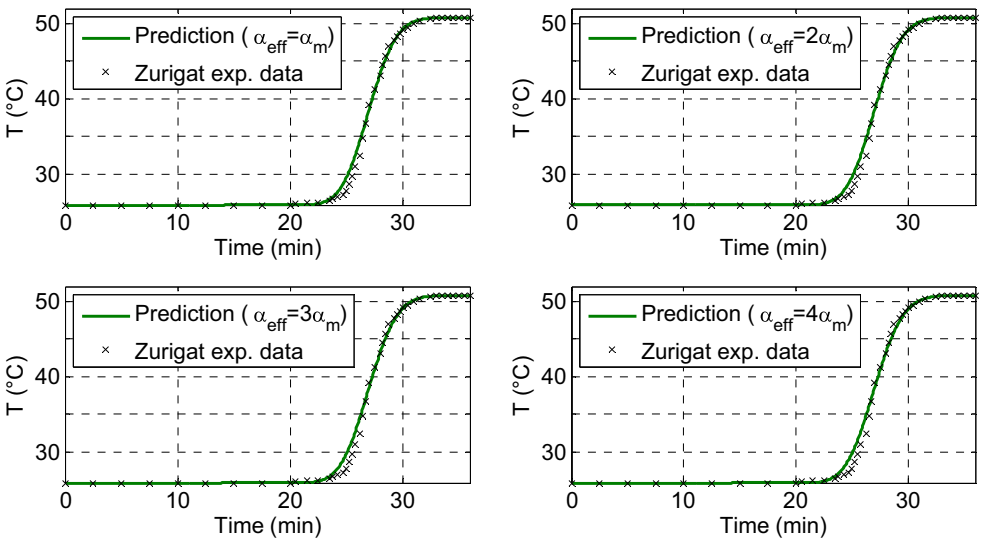

Fig. 5 Predicted temporal temperature development for different values of the effective thermal diffusivity at the outlet, location z = 1.22 m against Zurigat experimental data [2]

while in the region near the outlet the effective diffusivity equals the momentum diffusivity, i.e., the turbulent diffusivity is practically negligible.

The effect of thermal diffusivity reflects reasonably well the presence of turbulences caused by the mixing originating from the tank inflow. As the thermal diffusivity depends on the velocity, both will decrease with the height of the tank. Figure 6 presents the temperature profiles predicted by using the mixing length model proposed in the previous section and their comparison with the Zurigat experimental data and the predictions of the CIEMAT1D1SF model developed by Bayón and Rojas [2]; it can be observed that the prediction using the mixing length brings a marked improvement over that of CIEMAT1D1SF, when compared against the experimental data. However, the approach, although sound, does not intend to claim as being universal or free of some phenomenological limitations.

In cases (b) and (c), the implementation of the model to a packed-bed thermocline tank, the void fraction will have critical influence on the flow characteristics. Taking into consideration the porosity, the superficial velocity is much higher than that of the "free" flow. The proposed turbulence closure was not used because the inlet for these cases does not conform to the round impingement inlet condition because the inlet flow goes through a distributorv manifold. The behavior of the thermocline tank with both liquid and packed-bed as storage media is analyzed using the dimensions and properties of the materials of Sandia Laboratory prototype and the Solar One tank. Figure 7 presents the comparison of the predictions against the experimental data [15] for the Sandia Laboratory prototype.

The predictions, depite some modeling simplifications, such as temperautre-independent thermophysical properties, show very good agreement with the experimental data.

Figure 8 presents the comparison of the predictions against the Solar One experimental data [2]; the simulation is conducted by considering fixed thermophysical properties calculated

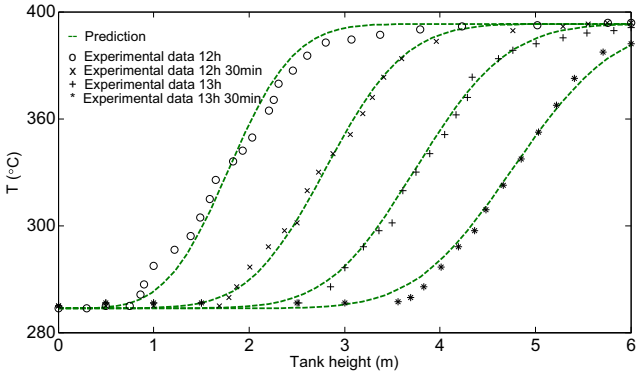

Fig. 7 Predicted temperature profiles variation with tank height at different times during a discharging process against the SL experimental data [15]

at mean averaged temperatures, and by taking the porosity for the monodisperse layers and for the mixture layer equal to 0.4 and 0.2, respectively.

By the observation of Fig. 8, it can be noted that the predictions, once again, show very good agreement with the experimental data with a maximum deviation of about 12%.

5 Conclusion

The proposed numerical model for thermocline tank, which relies on a time-implicit and non-iterative numerical solution, was developed and encoded within the Matlab environment. The model allows the comprehensive analysis of the transient charging/discharging phase. The mathematical formulation of the model is based on a single phase one-dimensional model, which allows the specification of the inlet temperature and velocity, physical properties, and initial conditions. The analyses of the thermal storage systems during the charging phase led to the following findings: the predictions agree well with the experiments in what concerns the time evolution of the

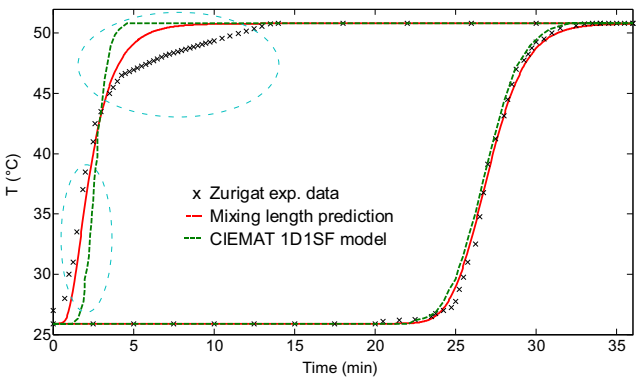

Fig. 6 Transient temperature profiles obtained by mixing length model and their comparison against the Zurigat experimental data and the model CIEMAT1D1SF predictions presented in [2]

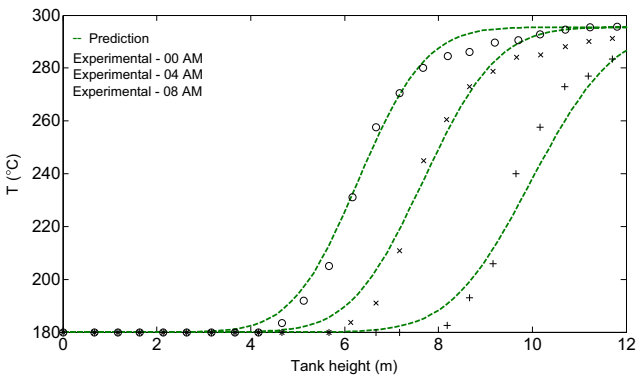

Fig. 8 Predicted temperature profiles variation with tank height at different times during the discharging process against the SO experimental data [2]

thermocline region. For impingement inlet condition, which generates high-level of turbulence in the vicinity of the impact region, is proposed a simplified algebraic turbulence closure, which leads to marked improvement of the predictions. This approach requires practically no additional computational effort and it relates, through the mixing length, the effective thermal diffusivity to the velocity profile of the fluid at each particular height of the tank. The tests for the thermocline tanks with packed-bed fillers indicate the predictions are in good agreement with the experimental data presenting a maximum deviation of less than 12%.

Acknowledgements The present work was sponsored by the State of Libya, under grant n° 469-2009.

References

1. González I, Lehmkuhl O, Pérez-Segarra C, Oliva A (2015) Dynamic thermoelastic analysis of thermocline-like storage tanks. Energy Procedia 69:850–859. https://doi.org/10.1016/j.egypro.2015.03.106
2. Bayón R, Rojas E (2013) Simulation of thermocline storage for solar thermal power plants: From dimensionless results to prototypes and real-size tanks. Int J Heat Mass Transf 60:713–721
3. Ehtiwesh I (2016) Exergetic, energetic , economic and environmental evaluation of concentrated solar power plants in Libya. http://ria.ua.pt/handle/10773/15882
4. Ehtiwesh I, Coelho M, Sousa ACM (2016) Exergetic and environmental life cycle assessment analysis of concentrated solar power plants. Renew Sust Energ Rev 56:145–155. https://doi.org/10.1016/j.rser.2015.11.066
5. Libby C (2010) Solar thermocline storage systems: preliminary design study. Report no. 1019581, EPRI, California
6. Tesfay M, Venkatesan M (2013) Simulation of thermocline thermal energy storage system using C. Int J Innov Appl Stud 3:354–364
7. Yang Z, Garimella S (2010) Thermal analysis of solar thermal energy storage in a molten-salt thermocline. Sol Energy 84:974–985
8. Yang Z, Garimella S (2010) Molten-salt thermal energy storage in thermoclines under different environmental boundary conditions. Appl Energy 87:3322–3329
9. Flueckiger S, Yang Z, Garimella S (2011) An integrated thermal and mechanical investigation of molten-salt thermocline energy storage. Appl Energy 88:2098–2105
10. Xu C, Wang Z, He Y, Li X, Bai F (2012) Sensitivity analysis of the numerical study on the thermal performance of a packed-bed molten salt thermocline thermal storage system. Appl Energy 92:65–75
11. Xu C, Wang Z, He Y, Li X, Bai F (2012) Parametric study and standby behavior of a packed-bed molten salt thermocline thermal storage system. Renew Energy 48:1–9
12. Xu C, Li X, Wang Z, He Y, Bai F (2013) Effects of solid particle properties on the thermal performance of a packed-bed molten-salt thermocline thermal storage system. Appl Therm Eng 57:69–80
13. Schumann T (1929) Heat transfer: A liquid flowing through a porous prism. J Franklin Inst 208:405–416
14. Zurigat Y, Liche P, Ghajar A (1991) Influence of inlet geometry on mixing in thermocline thermal energy storage. Int J Heat Mass Transf 34:115–125
15. Pacheco J, Showalter S, Kolb W (2002) Development of a Molten-Salt Thermocline Thermal Storage System for Parabolic Trough Plants. J So Energ Eng 124:153–159. https://doi.org/10.1115/1.1464123
16. Faas SE, Thorne L, Fuchs E, Gilbertsen N (1986) 10MWe solar thermal central receiver pilot plant: thermal storage subsystem evaluation – final report. Sandia National Laboratories, SAND86–8212
17. Mcmahan A (2006) Design & optimization of organic Rankine cycle solar-thermal power plants. Thesis, University of Wisconsin-Madison
18. Hoffmann J-F, Fasquelle T, Goetz V, Py X (2016) A thermocline thermal energy storage system with filler materials for concentrated solar power plants: Experimental data and numerical model sensitivity to different experimental tank scales. Appl Therm Eng 100:753–761. https://doi.org/10.1016/j.applthermaleng.2016.01.110
19. Murthy J (2002) Numerical Methods in Heat, Mass and Momentum Transfer. School of Mechanical Engineering, Purdue University, West Lafayette
20. Patankar S (1980) Numerical heat transfer and fluid flow. Series in coputational methods in mechanics and thermal sciences
21. Cushman-Roisin B (2014) Environmental fluid mechanics. John Wiley & Sons, Inc., New York
22. Wilcox D (2006) Turbulence Modeling for CFD, 3rd edn. DCW Industries, Inc., La Cañada
23. Van Driest E (1956) On Turbulent Flow Near a Wall. J Aeronaut Sci 23:1007–1011
24. Or C, Lam K, Liu P (2011) Potential core lengths of round jets in stagnant and moving environments. J Hydro Environ Res 5:81–91
25. Flueckiger S, Yang Z, Garimella S (2012) Thermomechanical Simulation of the Solar One Thermocline Storage Tank. J So Energ Eng 134:41014. https://doi.org/10.1115/1.4007665